Fizika Nizkikh Temperatur, 1996, v. 22, No 2, p. 140–157

Order and disorder in solid oxygen: neutron scattering investigations

F. Dunstetter and O. Hardouin Duparc

Laboratoire des Solides Irradiés, Ecole Polytechnique, F-91128 Palaiseau Cedex, France
E-mail:dunste@hp1sesi.politechnique.Fr

V. P. Plakhty

St.-Petersburg Nuclear Physics Institute, 188350 Gatchina, Russia

J. Schweizer

Centre d'Etudes Nucléaires, DRF/Sph-MDN, 85X, F-38041 Grenoble, France

A. Delapalme

Laboratoire Léon Brillouin, CEN Saclay, F-91191 Gif/Yvette Cedex, France

Solid oxygen exists at zero pressure in three crystallographic phases, denoted α, β, γ. Various results have been obtained by neutron scattering in the two disordered β and γ phases. Plastic γ-O_2 has a $A15$ structure with 8 molecules per unit cell. The molecules, located at $2a$ and $6c$ sites, exhibit two different types of disorder of molecular axes: a spherical-like disorder for the $6c$ molecules, and a disc-like disorder for the $6c$ molecules. A precise diffraction analysis on large single crystals shows that the disorder of molecular axis of the molecules can be interpreted in terms of localized forbidden orientations, or orientational holes, with a wide disorder among the other orientations. An important contribution of the translation-rotation coupling must be taken into account for the $6c$ molecules. Analysis of diffuse scattering by both an approximate analytical model and molecular dynamics simulation shows an important contribution to the orientational correlations between $6c$-$6c$ and $2a$-$6c$ molecules. Magnetic disorder can be investigated by neutron polarization analysis of the paramagnetic scattering. The $3D$ long range antiferromagnetic order of the α phase becomes a $2D$ short range helicoidal order in the β phase, with a very short 0.5 nm correlation range. In the γ phase, one observes, as in the liquid, a strong antiferromagnetic correlation, with a suggestion of a $1D$ order along the linear chains of $6c$ molecules. In all the measured phases, the variation of the scattering intensity with scattering vector $\mathbf{q}$ cannot be reproduced at high q by the known magnetic form factor. This suggests the need for a better description of the π orbital and the theoretical magnetic form factor of the molecule.

Introduction

The oxygen molecule is diatomic, with a magnetic moment arising from the presence of two unpaired electrons ($S = 1$) in a π orbital. As a result of the competition between orientational and magnetic disorder, there are three solid phases:

α-O_2 (temperature range $T < 24$ K, monoclinic) is antiferromagnetic;

β-O_2 (temperature range 24–44 K, rhombohedral) exhibits only a short range magnetic order;

γ-O_2 (temperature range 44–54 K, cubic) is both paramagnetic (disorder of the magnetic moments) and plastic (disorder of the molecular axes).

The structural, spectroscopic, and magnetic properties of solid oxygen have been extensively studied since the early forties, especially by the Ukrainian Kharkov group, at the origin of most of the pioneering results in spectroscopy and x-ray powder diffraction (see, e.g., [1] and references therein). But short-range order remained almost unexplored. Concerning the orientational disorder in the plastic phase, which needs single crystal investigations, the only results were two, x-ray (Jordan et al. [2]) and neutron (Cox et al. [3]), diffraction studies, which showed the presence of two sites with different types of disorder and proposed some models for the orientational disorder. Concerning the magnetic order and disorder, the antiferromagnetic structure of the α phase has been established in the sixties by neutron diffraction [4], and the magnetic diffuse scattering was already observed but remained uninterpreted until the pioneering work of Stephens et al. [5], who first inferred from neutron scattering experiments the inelastic behavior of the magnetic diffuse scattering in β-O_2 and proposed a triangular short-range order of magnetic moments in the hexagonal planes of the rhombohedral structure.

© F. Dunstetter, O. Hardouin Duparc, V. P. Plakhty, J. Schweizer, and A. Delapalme, 1996

We shall show in this paper how and why did neutron scattering make it possible a detailed experimental investigation of both orientational and magnetic disorder in the solid disordered phases, and as a result, forcing to question the theoretical interpretation of the experimental data. We shall also show that the solids made of diatomic molecules are probably among the few systems in which some unambiguous experimental results can be obtained for the orientational disorder.

The paper is organized as follows. The first part (Sections 1 and 2) is a discussion of some available results about the molecule itself and the experimental phase diagrams, staying within simple geometrical arguments and showing the special place of the oxygen system among the diatomic molecules. The known results show why we are interested to go beyond the averaged information on long-range order as obtained from crystallographic experiments and to measure directly the diffuse scattering associated with the short-range order, which can be more directly compared with spectroscopic results. The second part (Section 3) briefly reviews the fundamental and experimental features of the interaction between the neutron and the oxygen molecules which enable more detailed studies of the two types of short-range order observed in the disordered phases of oxygen. In the third part (Sections 4 and 5) we separately discuss the results of a study of the orientational disorder in the γ phase as well as of a study of the magnetic disorder in the β, γ, liquid, and gas phases.

1. The oxygen molecule: what can be measured with neutron scattering?

Prior to considering the phase diagrams in the next Section, we shall first recall the main properties of the molecule itself.

The molecule is diatomic ($d = 1.2074$ Å in the gas phase) with the electronic configuration

$$(1\sigma_g)^2(1\sigma_u)^2(2\sigma_g)^2(1\sigma_u)^2(1\pi_u)^4(3\sigma_g)^2(1\pi_g)^2 .$$

The three lowest energy states arising from the $(1\pi_g)^2$ configuration are $^3\Sigma_g^-$, Δ_g, $^1\Sigma_g^+$ within an ab initio calculation with atomic orbitals developed in Slater functions [6]. The ground state is $^3\Sigma_g^-$, and the others are higher in energy (respectively, 13120 cm^{-1} = = 18877 K and 21002 cm^{-1} = 30217 K). So, the only populated state at room temperature is the triplet state. Due to the large gap between the energy levels, the spin-orbit coupling remains very weak at room temperature and S is a good quantum number. The discrepancy between the experimental and calculated Lande factors $g_{exp} = 2.002089(16)$, $g_{calc} = 2.002064$ [7] and the free molecule factor $g_{free} = 2.00232$ has no effect on the solid properties. The energy splitting inside the spin triplet arising from the spin-spin ($\lambda_{ss} = 0.47$ cm^{-1}) and spin-orbit ($\lambda_{so} = 1.50$ cm^{-1}) couplings can be phenomenologically described by a S_z^2 term in the Hamiltonian, where $A = 4$ cm^{-1} = 5.8 K and z is the molecular axis. This energy separation can be neglected at the temperature of the experiments described below (40 to 65 K). For a compilation of spectroscopic data, see Ref. 8. The magnetic moment,

$$\mu = g[S(S+1)]^{1/2}\mu_B ,$$

can be ascribed to the triplet state, with $S = 1$ and $g = 2$. The magnetic form factor $f(q)$, discussed below, was calculated by several authors [9–11] by representing the π orbital as a combination of the $2p$ atomic orbitals of the two oxygen atoms:

$$\pi_g^{\pm} \approx 2p_{\pm} - 2p'_{\pm} .$$

The total electron density has an axial symmetry $D_{\infty h}$ [12] and the homonuclear molecule has no dipole moment. The first nonzero term of the electrostatic energy development is a quadrupole moment of $Q = -0.39 \cdot 10^{-26}$ esu·cm^2 [13], four times weaker than that of the N_2 molecule.

Ab initio calculations show [14] that the exchange interaction between the molecules is direct, with a very fast (R^{-14}) radial decay. The ab initio exchange energy can be represented by a Heisenberg term $-J\mathbf{S}_1\mathbf{S}_2$, but the exchange integral J strongly depends on the relative orientation of the molecules. The coupling is antiferromagnetic in most of the cases but can become ferromagnetic in some cases. This latter point, which remains controversial and questionable [15] and does not appear in most of the experimental results, giving fairly isotropic physical properties, may be due to molecular disorder.

The interactions between molecules are usually described by a phenomenological Lennard-Jones potential, whose parameters are refined on various physical properties [16], combined with a quadrupolar contribution and, in the case of oxygen, a magnetic Heisenberg term, which is rather small in the 50 K temperature range. What is important in the case of oxygen (and fluorine) and developed in the next Section, is that the quadrupolar term is small, leading to a phase diagram quite different from the one for other diatomic molecules. We shall show in the next Section that the relevant parameter is the relative strength of the van der Waals and quadrupolar interactions.

As will be seen in Sec. 3, the π orbital carrying the unpaired electrons is responsible for the magnetic interaction with a neutron that produces a magnetic scattering of the neutron by the molecule, directly related to the magnetic form factor of the molecule,

i.e. the Fourier transform of the π orbital. The measurement of this scattering thus provides an experimental tool for obtaining results that can be directly compared with quantum chemistry calculations.

Due to the weakness of the magnetic interaction, as compared to the van der Waals term, the magnetic and orientational problems can be treated separately. In the paramagnetic and plastic γ phase, disordered in two ways, the magnetic interaction is negligible and the orientational problem can be understood without any magnetic consideration. But the presence of the magnetic moments yields additional experimental information, which greatly helps to understand the nonmagnetic scattering results by enabling an independent determination of the distance between the molecules, especially in the liquid phase.

2. Oxygen among the diatomic molecules: the phase diagrams

In this Section we discuss the results available in the literature, showing the special place of oxygen among the diatomic molecules, and the interest of a better knowledge of the local orientational disorder in its plastic phase.

2.1. Long range order

The high pressure phase diagrams have been determined by x-ray scattering since the seventies, especially by the Los Alamos group [17]. The diamond anvil cell techniques have been continuously improved, the discovery of new solid phases of the diatomic cryocrystals closely following the technical progress. The *PT* phase diagrams of O_2 (Olinger et al. [17]) is shown in Fig. 1; those for N_2 and CO (Mills et al. [17]) — in Fig. 2; the zero-pressure diagram of F_2 — in Fig. 3 (Jordan et al., Meyer et al. [18]). Due to extreme experimental difficulties with F_2, no high pressure results have been as yet published to our knowledge. The NO molecule is not considered here, since it is no more diatomic in the condensed phase: one observes a dimerization in the liquid and solid phases, so that paramagnetic NO molecules form diamagnetic dimers in the condensed state.

One clearly observes two classes of solid compounds: the (O_2–F_2) group, on the one hand, and the (N_2–CO) group, on the other hand, O_2 and CO being the extreme cases.

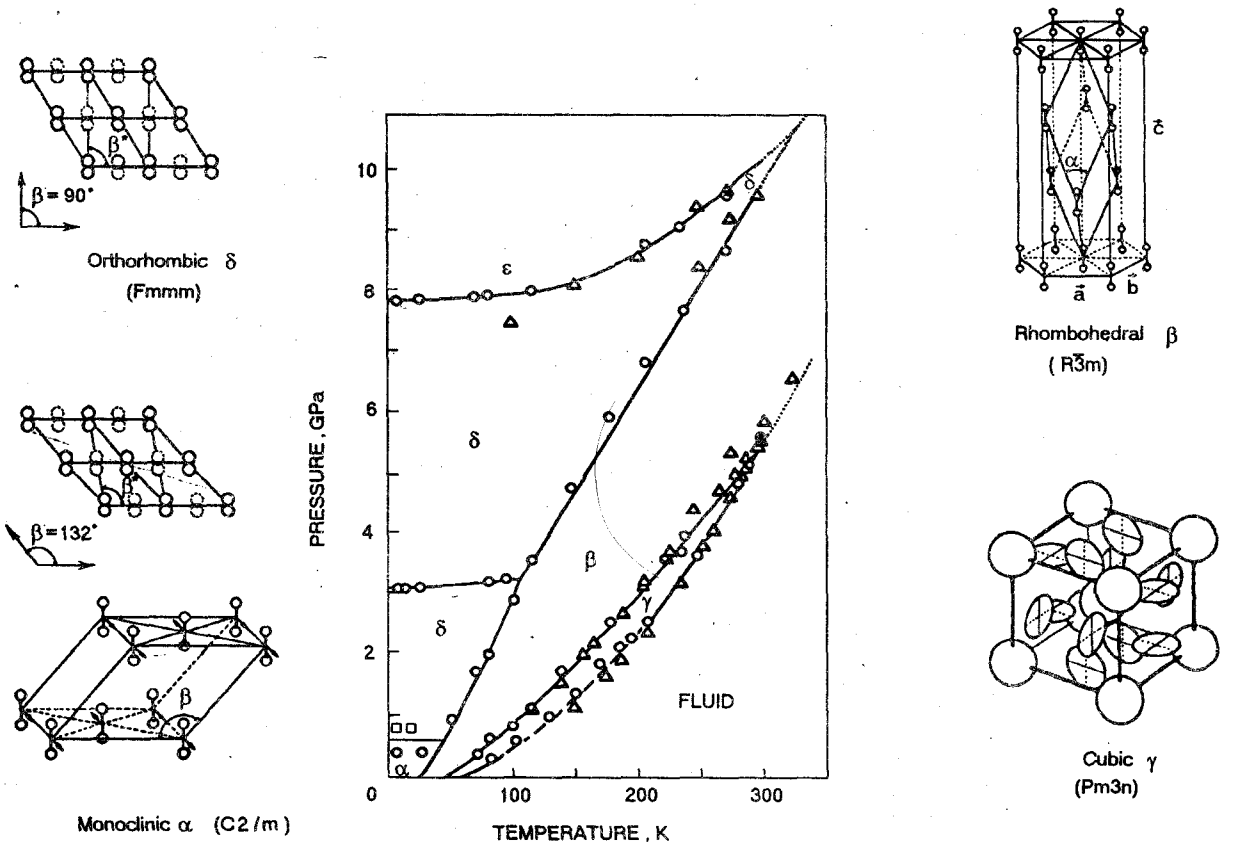

Fig. 1. PT phase diagram of oxygen [17]. The only orientationally disordered phase is the γ phase.

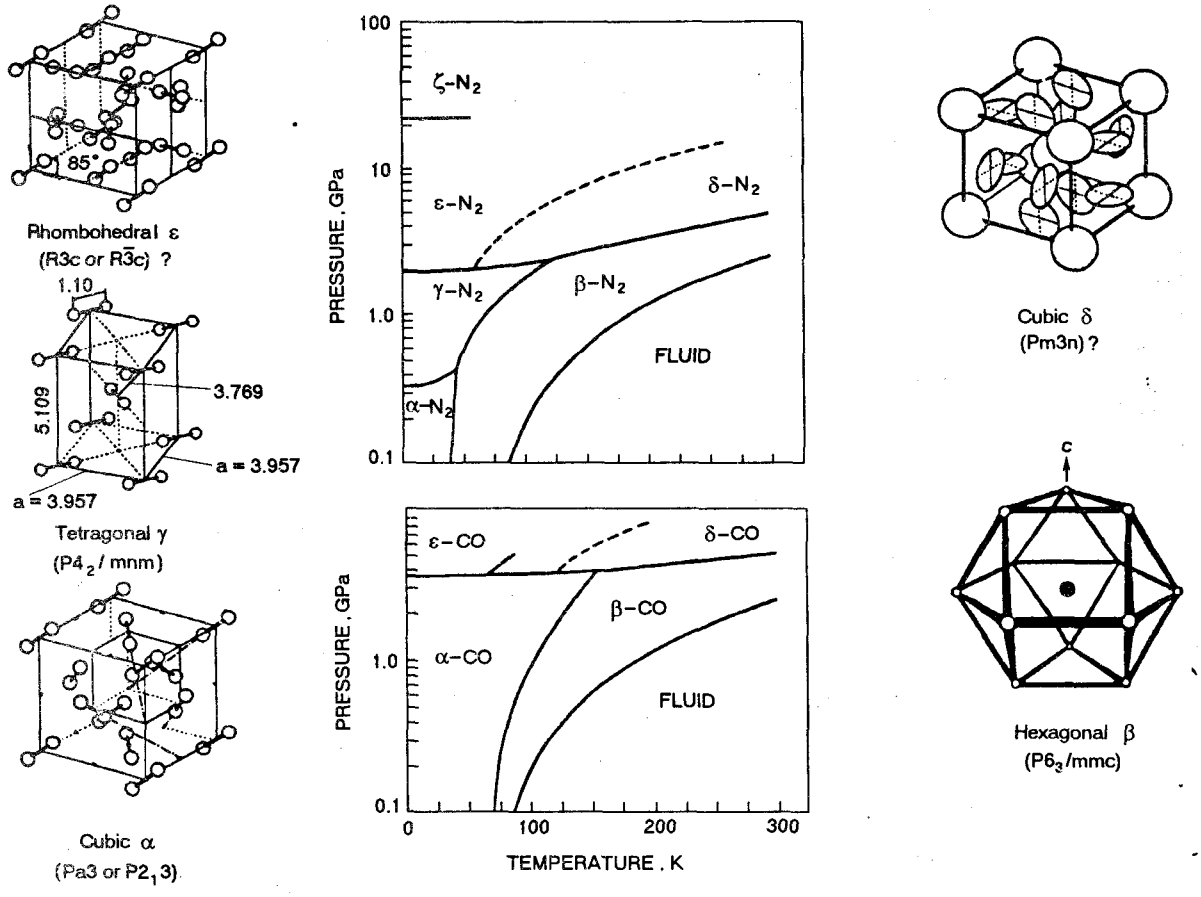

Fig. 2. PT phase diagram of nitrogen and carbone monoxide [17]. The β and δ phases are orientationally disordered. The α, γ, ε phases are orientationally ordered.

For the $(O_2$–$F_2)$ group, one observes a cubic *A15* plastic structure at zero pressure, with two distinctly different types of disorder: two molecules (2*a* sites) at the corners and centre of the unit cell have a quasi-spherical disorder while the six other molecules (6*c* sites), located on the faces of the cube, have a disc-like disorder: they stay within a plane during their rotation, which allows them to be at closer contact while being disordered. These disc-like molecules form chains along three equivalent axes of the crystal, similar as observed in the V_3Si-type superconductors. The spherical-like molecules occupy empty space between these chains. The plastic phase of oxygen disappears at high pressure.

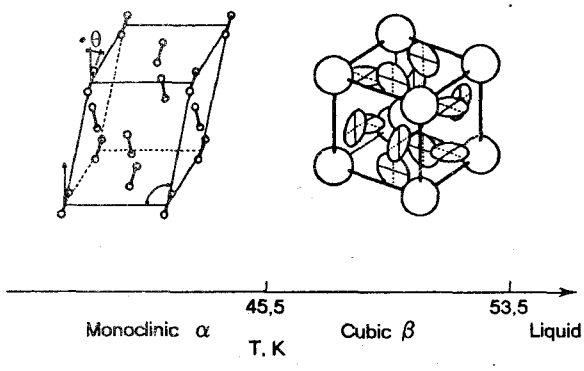

Fig. 3. Phase diagram of fluorine at zero pressure [18].

The various ordered phases can be considered as some variations of the basic monoclinic structure, with the planes of molecules parallel to each other, and parallel to the reciprocal axis c^*. The distance between these planes remains almost constant, developing a deformation within the (a,b) plane, which leads to the rhombohedral β-O_2 and orthorhombic δ-O_2 phases for special values of the in-plane deformation angle and the monoclinic angle β, respectively.

For the $(N_2$–$CO)$ group, a plastic phase at zero pressure is also observed, but here the structure is hexagonal, with only one type of orientational disorder. The ordered phase is cubic, with a fcc arrangement of the centres of mass of the molecules and the molecules, oriented along the $\langle 111 \rangle$ directions of the

cubic unit cell. The most striking result is that a completely different phase diagram is observed at high pressure (with the same *A15* structure) than for the $(O_2$–$F_2)$ group. The low temperature high pressure rhombohedral ε phase is a slightly distorted version of the *A15* structure. In the intermediate-pressure δ phase, the nearest-neighbor molecules (corner and centre of the tetragonal cell, distance 3.79 Å) remain orthogonal, and the second neighbors (distance 3.96Å) form planes of parallel molecules.

These phase diagrams can be related in a very simple way to the fundamental molecular features previously described, if one notices that the O_2 molecules do their best to be parallel and to escape the orthogonal mutual orientation, whereas the N_2 and CO molecules do their best to be orthogonal to each other, thus obeying their strong quadrupolar interactions. But at high pressure, the balance is modified to the favour of the repulsive exchange interaction and the influence of the quadrupolar interaction becomes smaller and smaller, finally leading again to the *A15* structure. The quadrupolar interaction energy varies as Q^2/R^5 and the Q^2 values are 0.16, 0.42, 1.5, 4 (in 10^{-52} esu$^2\cdot$ cm^4 units) for O_2, F_2, N_2, CO, respectively, which shows the extreme situation of oxygen.

So we come to the very simple idea that the *A15* phase is experimentally shown (by all the above crystallographic results) to be the stable orientationally disordered phase of a system of pure quasi-van-der-Waals diatomic molecules, with O_2 as the model compound. At the opposite, the hcp phase is the stable orientationally disordered phase for diatomic molecules with strong quadrupolar interaction, with N_2 as the model compound.

As to the ordered phases, the competition between the Lennard-Jones and the quadrupolar components of the interaction potential was already discussed by English and Venables [19] a long time before (1974) the publication of the high pressure results. They showed that the low-temperature cubic α-N_2 phase and the rhombohedral β phase of O_2 (with a transition towards a monoclinic one with increasing d/σ) were the stable phases respectively for strong and weak quadrupolar interaction in the ordered state. This is clearly confirmed by experiment.

Since our main interest in the orientational problem is the plastic disordered phase, we shall restrict the discussion to the *A15* and hcp plastic phases.

2.2. *Short range order*

Always adhering to simple considerations, it is now interesting to pass from the long range structure obtained by crystallographic experiments to the short range order. Consider a molecule surrounded by twelve neighbors, all the nearest heighbors in the case of the hcp structure or twelve 6*c* molecules around a central 2*a* molecule in the *A15* array. Let ρ_1 be the distance between the central molecule and each of its twelve neighbors (*A15*: 2*a*-6*c* distance), ρ_2 and ρ_3 be the two possible distances between the surrounding molecules (*A15*: 6*c*-6*c* distances). Textbooks show that it is possible to pass continuously from an *A15* structure to a fcc structure, with an intermediate very symmetric icosahedral short range order, by simply deforming the rectangle formed by four coplanar neighbors and the central atom. The 3*D* structure is obtained with the C_3 rotations defining the cubic structure. The only parameters are ρ_2/ρ_1 and the density. The hcp structure is obtained from the fcc structure by a simple rotation through 60° of a set of three molecules having a common C_3 axis that becomes the C_6 axis, thus loosing the cubic symmetry. But the difference between fcc and hcp concerns much larger distances: for the nearest-neighbor short range order considered here, the hcp and fcc 13-molecule clusters are quite equivalent. The calculated values of the ratios ρ_2/ρ_1 and ρ_3/ρ_1 are 0.894 and 1.095 for the *A15* cluster, 1.051 and 1.051 for the icosahedral cluster, 1.414 and 1.000 for the fcc and hcp clusters. We see a complete inversion between *A15* and hcp clusters: the molecules can approach much closer in the *A15* structure, thereby allowing the strange disc-like disorder experimentally observed, with the cluster structure close to icosahedral geometry. At the opposite, all molecules have the same environment in the hcp phase.

It must be noted that in the icosahedral case, all the distances between nearest neighbors are the same, as in hcp, but with a completely different local order, very close to the *A15* local order.

Several experimental results support the idea that such an icosahedral structure probably exists in liquid oxygen and experiments are in progress. The very low vapor pressure in equilibrium with the solid indicates a close similarity of the local orders [20] in the liquid and the plastic solid. Our magnetic diffuse scattering data are rather similar for the liquid and the *A15* phase and the distance between antiferromagnetically correlated molecules is just the same, whereas the splitting of the stretching Raman line discussed by many authors [21] shows clearly two distinct sites of the *A15* structure and only one type of site in all other liquid and solid phases. Thus, at the melting transition, the local order clearly changes, as indicated by Raman data, but the change is small as indicated by thermodynamics and magnetic scattering.

In conclusion of this state of the available crystallographic results, interest to study the nature and details of the short range order is now clearly rekindled. These can be a support to any theoretical

study based on energy or force calculations either implying a priori models of mutual arrangement of these molecules, or evaluating such arrangements with simulations.

Oxygen can be considered as the simplest case of quasi-pure van der Waals system with respect to orientational order or disorder. At the opposite side, nitrogen can be considered as the model system for strong quadrupolar coupling. This has been known for a long time for nitrogen, which is traditionally taken as the examplary diatomic compound. Oxygen, often considered as approximately equivalent to nitrogen, is abandoned because of the larger experimental difficulties. We have seen that the notion of this similarity is not always true.

3. Oxygen and neutron scattering

The most evident drawback of neutron scattering is the need for a nuclear reactor to produce them and, in view of the necessity to measure weak signals, the poor flux of the available sources. But proceeding from the nature of the interaction between neutrons and matter (in our case, between the neutron and the oxygen molecule), several good reasons arise to choose this radiation for diffuse scattering experiments and diffraction investigation of the disordered phases of oxygen. Some of these reasons will appear below. The most evident one is the magnetic interaction.

As shown in the previous Sections, the interesting problems for neutron experiments are:

— paramagnetic scattering related to the electronic structure of the molecule itself;

— diffuse magnetic scattering related to the magnetic Heisenberg interaction between the magnetic moments of the molecules;

— nonmagnetic diffraction and diffuse scattering due to the orientational order or disorder and related to the intermolecular forces.

Let us now comment on the neutron-molecule interaction itself, which makes these studies possible, and several consequences for the practical realization of the experiments. We first discuss some implications of the nuclear interaction between neutron and nuclei of the atoms for the experiments described in Sec. 4. Then we describe the general features of magnetic scattering as well as the polarization analysis experiments we used for the experiments described in Sec. 5.

3.1. Nuclear scattering

In a nonmagnetic system, the neutron interacts with the nuclei of the atoms, which are treated as points on the scale of interatomic distances. The usual atomic form factor of x-rays, which damps the measured signal at high scattering angles, is here replaced by the angle-independent coherent diffusion length b. This allows a better measurement at higher angles, where weak diffraction lines carry significant information on the disorder in a single crystal experiment as the one described in section 4.1. Since the interaction of matter with neutrons is much weaker than with x-rays, the absorption is rather low, and a neutron beam can travel a few centimeters of matter before it is absorbed. This allows experiments to be done far from room temperature with rather simple sample cells, which would be either impossible or very difficult in the conditions of a x-ray experiment with a standard x-ray diffractometer, due to the additional complication for the beam of beryllium or Mylar windows. It is more so in high-pressure or low-temperature experiments as is the case with the cryocrystals. The flux from the actual synchrotron sources is so high that the absorption problem could be considered as less important, but the experimental conditions of a synchrotron, with the beam under high vacuum, the high flux of radiations and the large dissipation in the sample makes the use of synchrotron radiation for cryocrystals still rather unrealistic or very difficult. In the case of neutrons, the sample environment is simpler, considering both the «living conditions» for the experimentalists near the beam (no vacuum, rather low level of radiations, and much simpler biological protection against radiation injury) and, consequently, the design of the cryostat.

As an example we can mention the thermal design of our cell for in-situ growth of large single crystals needed to study the oxygen γ phase (see Sections 4.1 and 4.2). The ability of neutrons to cross anything allowed a much simpler cell design than in the case of x-rays. Thus, simple analytical models were a good help in the successful optimization [22] of the cell, yielding a completely reliable growth method.

Nevertheless, all these advantages of neutrons can be counterbalanced by the need of large samples of a few cm^3, which is sometimes impossible for single crystal experiments. This is one of the most important reason why experimental studies of molecular disorder from diffuse scattering remain scarce: it is often impossible to grow large enough single crystals free from any spurious crystallites, which is necessary for an unambiguous indexing of the scattering in reciprocal space, prior to any analysis of the data.

3.2. Magnetic scattering

The theory of magnetic scattering was first developed by Halpern and Johnson [23] and the first experimental polarization analysis spectrometer was built in Oak Ridge by Moon et. al. [24].

The interaction between a neutron and a magnetic atom can be described by the operator

$$U = A + Bs \cdot \mathbf{I} - ps \cdot \mathbf{S}_{\perp}$$

acting on the two eigenstates of the S_z operator, $|+\rangle = |1/2, 1/2\rangle$ and $|-\rangle = |1/2, -1/2\rangle$, of the neutron spin s, represented by the Pauli matrices. Here I is the spin operator of the nucleus; S is the electronic spin operator; $S_\perp$ is the active part of the electronic spin, i.e. the component of S normal to the scattering vector q ($S \sin\alpha$, where α is the angle S makes with q); A and B are two constants chosen so as to match the experimental scattering lengths b^+ and b^-, measured in the $|+\rangle$ and $|-\rangle$ states. After averaging the matrix elements of $(A + Bs\cdot I)$ over nuclear spins one can obtain the matrix elemtnts of U (see below) as a function of the neutron state. Now, p is a function of q, namely $p = \Gamma g f(q)$, where $\Gamma = \gamma r_0/2 = 0.2695\cdot 10^{-12}$ cm, $\gamma = -1.913$ is the gyromagnetic ratio of the neutron and r_0, the classical radius of the electron. The magnetic form factor

$$f(q) = \int dr\, e^{iq\cdot r} \rho_{spin}(r)$$

is the Fourier transform of the spin density.

The $sS_\perp$ term depends on the mutual orientation of the three vectors s, S and q which can be chosen by the experimentalist in most cases: s and q depend on the geometry and the design of the spectrometer, and S can be chosen for some samples (e.g. a ferromagnetic compound in saturating field). This allows a great variety of differential methods, all based on the constant value of the nonmagnetic scattering for two geometries of these three vectors, for which the magnetic term changes sign. The geometry is chosen so as to maximize the magnetic signal as compared to the other contributions, which are to be subtracted.

Four diffusion amplitudes (the matrix elements of U) can be defined for the four possible transitions of the neutrons:

$$U^{++} = b + BI_z - pS_{\perp z}\,,$$

$$U^{+-} = B(I_x + iI_y) - p(S_{\perp x} + iS_{\perp y})\,,$$

$$U^{-} = b - BI_z - pS_{\perp z}\,,$$

$$U^{-+} = B(I_x - iI_y) - p(S_{\perp x} - iS_{\perp y})\,,$$

U^{++}, U^{-} are called «non-spin-flip» amplitudes since they leave the neutron spin unchanged; U^{+-}, U^{-+} are the «spin-flip» amplitudes since they change the neutron spin state; b and B are the coherent and incoherent lengths.

The principle of a polarization analysis spectrometer is to analyze each of these amplitudes by choosing the polarization of the incident beam using the first polarizing monochromator and the precession coils, which sets the $|+\rangle$ or $|-\rangle$ incident state of the neutron, and then measuring either spin-flip or non-spin-flip component of the scattered beam with another analyzing crystal. Combined with the vectors arrangements described above, this method proved to be very efficient to measure weak magnetic signals. The setup depends on the physical problem to be studied. Because of the three successive diffusions and the double polarization filtering between the reactor and the counter, the experiments are rather long and cannot be routine.

The usual nuclear scattering discussed in the previous paragraph depends on b and is purely non-spin flip. Therefore, it is very easy to eliminate it by simply choosing a spin-flip setup. The incoherent nuclear scattering, which only produces a constant background, has either a spin-flip or a non-spin-flip component, and a differential experiment must be performed to separate it from the magnetic scattering.

In our case, the system is paramagnetic, and we did not try to align the moments, which should need a very high magnetic field. It is much easier to place two perpendicular magnetic coils around the sample, producing either a horizontal field parallel to the scattering vector or a vertical field normal to the scattering vector. These (weak) fields determine the polarization σ of the neutron in the sample. In this geometry, the spin-flip (sf) and non-spin-flip (nsf) intensities are

$$I_H^{sf} = I_{magn} + 2/3 I_{incoh\ nucl}\,, \quad I_H^{nsf} = 0\,,$$

$$I_V^{sf} = 1/2 I_{magn} + 2/3 I_{incoh\ nucl}\,,$$

$$I_V^{nsf} = 1/2 I_{magn} + 2/3 I_{incoh\ nucl}\,,$$

where the index H or V is the direction of the field.

So, in both cases the magnetic intensity can be directly obtained from a differential measurement:

$$1/2 I_{magn} = I_H^{sf} - I_V^{sf} = I_V^{nsf} - I_H^{nsf}\,.$$

Choice of spin-flip or non-spin-flip conditions depends on what one wants to measure. In our case we wanted to measure the magnetic diffuse scattering which is very weak compared to the intense Bragg lines of the solid. Now, as the nuclear Bragg lines are purely non-spin-flip, they will be completely eliminated by a spin-flip setup.

4. Orientational order and disorder in the plastic γ phase

Before starting the investigation of the diffuse scattering, showing between the Bragg peaks, we preliminarily re-examined the mean line structure in the conventional moving-arm single crystal diffrac-

tion experiments, discussed in Sec. 4.1. Then the diffuse scattering experiment, described in Sec. 4.2, was performed and an analytical model was developed in order to improve the standard approximation, neglecting the correlations between the molecules, which is clearly wrong in our case. This approximation is not sufficient to provide a proper description of the scattering measured, so we recently started Molecular Dynamics simulations to overcome the limitations of the analytical model. First results are presented here and some problems found when comparing experimental data with numerical or theoretical calculations are discussed.

In this Section we shall not enter into details of the formalism, which are rather cumbersome owing to the two types of sites and the numerous models of disorder. These details will be reported elsewhere. We would rather discuss here the historical context, the general ideas behind these models, and the problems we are facing in the interpretation of such an experiment.

4.1. Standard crystallographic experiment

The *A*15 structure was first inferred by Jordan et al. [2] from x-ray diffraction data. Various models of continuous or statistical disorder were tested, but it was not possible to choose between these models. The later neutron diffraction study by Cox et al. [3] favoured stastistical models with the 2*a* spherical-like molecules oriented along ⟨111⟩ directions of the cubic cell and two different models for the orientation of the 6*c* disc-like molecules. But some contradictions between the refined parameters made difficult the choice of the parameters needed for the interpretation of the diffuse scattering data.

So, we preferred to perform this experiment again [25]. Our experimental results are fully consistent with Cox's experiment [3]. However, due to the important evolution of the knowledge of molecular systems and the models used for the analysis of the data in the period between the two experiments, our analysis was quite different from the one of Cox et al.

In the early seventies, statistical models were used as the standard tool for the description of molecular orientational disorder. The seventies and eighties saw an explosion of the multipolar expansion analysis, made popular in the community of molecular crystallography by a series of papers of Hüller and Press [26]. Multipolar expansions were introduced by Von der Lage and Bethe [27] for solid state problems and widely studied in the sixties by Altmann with coworkers [28]. These methods were also developed by the groups in Buffalo (P.Coppens et al. [29]) and Helsinki (Kurki-Suonio et al. [30]) for nonspherical charge distributions. This multipolar analysis was an important factor of the wide development of diffraction analysis of molecular systems. Concerning our problem, however, one of the results of this period is that complex rotational symmetries have been found, which showed the limitations of the statistical models. The first problem to appear in the mid-eighties was with some highly disordered systems for which centres of mass of the molecules move when the molecules rotate. This rotation-translation coupling is rather difficult to introduce in the multipolar formalism. There was an attempt [31] to introduce such a displacement of the centre of mass with a Taylor expansion of the rotational probability distribution function around the mean position of the centre of mass. But rather obscure parameters are thus introduced, which do not really enlighten the underlying physical problem.

Faced both with such an evolution of the molecular analysis and with a compound with high disorder, low symmetry (two sites, one of them of noncubic symmetry) and too few experimental data to fit the proper multipolar expansions, we had to go back to the old statistical models. We investigated numerous sets of orientations, introduced in the refinement via statistical models, just as an intermediate tool to simulate the multipolar expansion process, and not as a final model. A lot of different sets of orientations produced the same refinements. The conclusion is that it is not possible to define a precise set of orientations for the molecules (e.g., the ⟨111⟩ orientations), but some sets of orientations were clearly excluded, which can be interpreted as forbidden orientations or orientational holes.

The spherical-like 2*a* molecules are highly disordered, so the fully spherical model could not be excluded. Nevertheless, the ⟨100⟩ orientations were always unfavorable, as well as the ⟨120⟩ ones, in the direction of the 6*c* neighbors. This can be interpreted as a quasi-free rotation of the 2*a* molecule, which simply avoids the unfavourable orientations. For the 6*c* disc-like molecules, a continuous cylindrical disorder is clearly excluded. The refinement diverged for all the models with the 6*c* molecules within 2° in the vicinity of the ⟨100⟩ and ⟨110⟩ orientations (within the disc) and was equally successful for any other orientation. This can be interpreted as a wide libration inside angular sectors 35° to 40° wide, with jumps between these sectors on the time scale (10^{-13} s) of the neutron interaction with the molecule.

Another important result is the dramatic effect of the introduction of a translation-rotation coupling in the refinement process. For the same sets of orientations, the crystallographic residue decreased from about 7.5 %, which is the usual result for standard multipolar analysis, down to 2.5 or 3.5 %, depending on the orientation, which we consider as the experimental limit of our analysis related to geometry of the diffractometer and the crystal. This model, where the 6*c* molecules move along the axis perpendicular to their rotation plane in order to escape the 2*a* neigh-

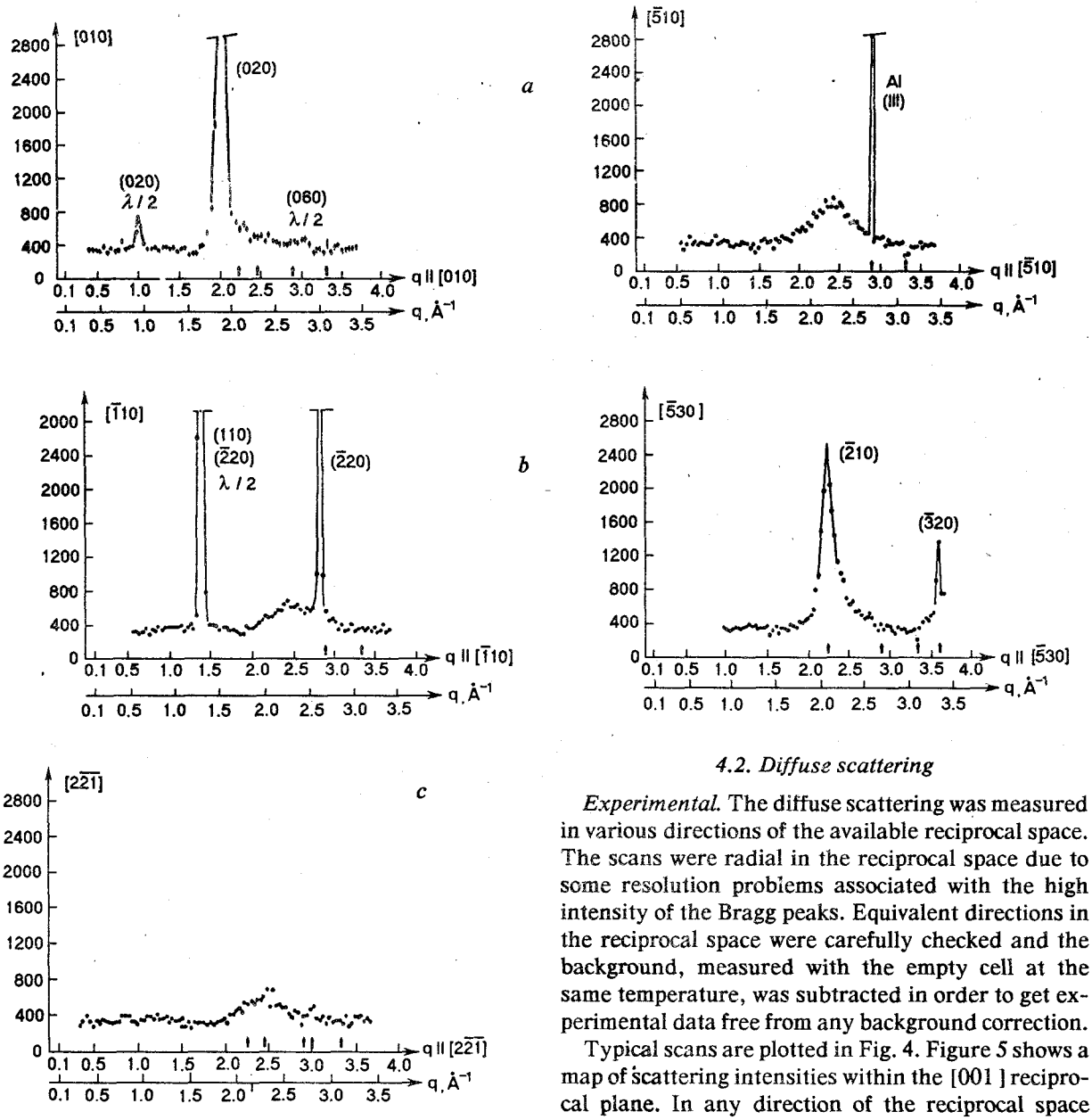

Fig. 4. Total nuclear neutron scattering: typical scans in interesting directions of the reciprocal space. The background has been subtracted. The error bars, indicated on the [010] scan, are the same for all other scans. Both $\mathring{A}^{-1}$ and $a^* = 2\pi/a$ ($a = 6.78$ Å) wavenumber units are indicated on the horizontal axis. The arrows above the horizontal axis indicate the position of subtracted Bragg lines from the sample environment.

bors, is fully confirmed by numerical analysis of the energy of clusters of molecules.

The advantage of our approach is to have been able both to obtain the same type of results as with the multipolar expansion for the orientational disorder, and to allow the introduction of translation-rotation coupling in a simple way, with a physically understandable parameter.

4.2. *Diffuse scattering*

Experimental. The diffuse scattering was measured in various directions of the available reciprocal space. The scans were radial in the reciprocal space due to some resolution problems associated with the high intensity of the Bragg peaks. Equivalent directions in the reciprocal space were carefully checked and the background, measured with the empty cell at the same temperature, was subtracted in order to get experimental data free from any background correction.

Typical scans are plotted in Fig. 4. Figure 5 shows a map of scattering intensities within the [001] reciprocal plane. In any direction of the reciprocal space (except [100]) we observe a diffuse peak with the maximum at the same value $q = 2.3$ $\mathring{A}^{-1}$, where q is defined as $q = 4\pi \sin\theta/\lambda$. This scattering is very similar to the one observed in the liquid, but with a lower intensity. It is modulated in the reciprocal space with a broad maximum around the [100] directions and a sharp minimum just in these [100] directions. What we have measured in such an experiment is the total scattering of the system, since we made no experimental analysis of any parameter. This is what can be in principle directly compared to a numerical simulation of the scattering.

General formalism. The experimental data can be separated into two contributions: the Bragg contribution, discrete and located at the reciprocal lattice

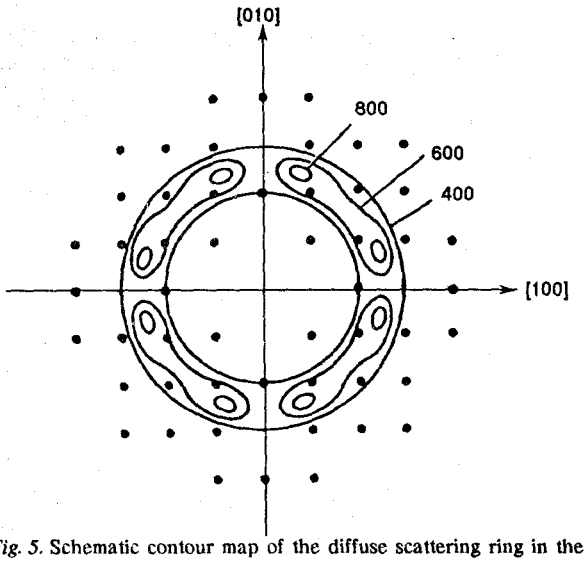

Fig. 5. Schematic contour map of the diffuse scattering ring in the [001] reciprocal plane.

sites, and the diffuse contribution, continuous and distributed everywhere in the reciprocal space:

$$I_{exp}(\mathbf{q}) = I_{Bragg}(\mathbf{q}) + I_{diffuse}(\mathbf{q}) .$$

The Bragg contribution is nothing but what was treated in the previous Section.

Introducing the normalized intensity $S(\mathbf{q})$, the calculated intensity is given by (see, e.g., Dolling et al. [32])

$$I(\mathbf{q}) = NS(\mathbf{q}) = \langle \sum_{uij} \sum b_i b_j^* \, e^{i\mathbf{q}\cdot(\mathbf{r}_i - \mathbf{r}_j)} \rangle ,$$

where the summations run over all the pairs i, j of atoms in the crystal; b_i is the diffusion length of atom i located at position $\mathbf{r}_i$ in the crystal. The $\langle ... \rangle$ means averaging over the disorder of the system.

A direct calculation is always possible using the Molecular Dynamics or Monte Carlo methods, but the main interest is not to calculate this expression but to get an insight into the nature of the disorder in the system. Therefore, this expression must be split in several terms associated with various contributions of the disorder to which physical meaning can be attributed. The formalism outlined below can be summarized as follows. The first step is to transform the ensemble of atoms into an ensemble of molecules for which one must introduce an internal structure and, thereby, a molecular form factor. The rigid block approximation allows the separation of translational and rotational degrees of freedom in clear cut terms. Finally, correlations between these degrees of freedom are considered to consitute the basis for the final separation of the total scattering.

In the rigid block approximation, each atom i can be ascribed to a given molecule m, so one can replace the index i by the set (m, a). Then one divides the instantaneous position $\mathbf{r}_i$ of the atom i into three terms:

(i) the constant part $\mathbf{R}_m$ of the translational degree of freedom of the centre of mass of the molecule (the crystallographic site);

(ii) the varying part $\mathbf{u}_{m,a}$, i.e. the instantaneous displacement of the centre of mass from the above mean value (including both the high frequency vibrations of the atoms and the slower global translations);

(iii) the relative position $\mathbf{x}_{m,a}$ of the atom with respect to the center of mass, i.e. the rotational degrees of freedom.

By replacing $\mathbf{r}_i$ in the previous formula by

$$\mathbf{r}_i = \mathbf{R}_m + \mathbf{u}_{m,a} + \mathbf{x}_{m,a} = \mathbf{R}_m + \mathbf{u}_m + \mathbf{x}_{m,a} ,$$

where the rigid molecule approximation allows us to ascribe the shift $\mathbf{u}_{m,a}$ to the whole molecule and to replace it by $\mathbf{u}_m$.

One defines a translation factor $T_m(\mathbf{q})$ which includes the varying part of the translational degrees of freedom of molecule m, and the normalized rotational form factor of the molecule, $\beta(\mathbf{q})$, which takes into account the geometry of the molecule:

$$T_m(\mathbf{q}) = e^{i\mathbf{q}\cdot\mathbf{u}_m} ,$$

$$\beta_m(\mathbf{q}) = \frac{\sum_a b_a \, e^{i\mathbf{q}\cdot\mathbf{x}_{m,a}}}{\sum_a b_a} ,$$

where the summation runs over all the atoms a of a given molecule and $\beta_m(\mathbf{q})$ includes all the rotational degrees of freedom of molecule m,

$$\beta_m(\mathbf{q}) = \cos(\mathbf{q}\cdot\vec{\delta})$$

for such a homonuclear molecule as oxygen ($\vec{\delta}$ is half of the internuclear distance). The case of the liquid is included in these expressions, since it is just the case where $R_m = 0$ for all the molecules.

The previous expression becomes

$$S(\mathbf{q}) = \langle \sum\sum \beta_m^* \beta_n T_m^* T_n \, e^{i\mathbf{q}\cdot(\mathbf{R}_m - \mathbf{R}_n)} \rangle ,$$

where the summations now run over all molecules m and n in the crystal.

One splits this expression to distinguish between the intramolecular (single particle rotation: $m = n$) and intermolecular (correlation: $m \neq n$) terms:

$$S(\mathbf{q}) = S_{intra}(\mathbf{q}) + S_{inter}(\mathbf{q})$$

or

$$S(q) = S_{single}(q) + S_{corr}(q) .$$

Both notations can be found in the literature. But the latter one is ambiguous because both terms involve correlation terms, the only difference being the location of the relevant atoms.

The intramolecular term is a single-particle term, which only depends on the rotation of an individual molecule. It is easy to calculate analytically for reasonable models. This is the major contribution to the diffuse scattering. The second term is very difficult to calculate and the usual approximation is to neglect it. Since both terms involve distances between atoms, they are generally oscillating functions in the whole experimental range. For molecules with van der Waals radii of $\sigma \approx 3$ Å, the first correlation peak appears for atoms of neighboring molecules at close contact at $q \approx 2\pi/\sigma \approx 2.1$ Å^{-1}. This value is consistent with our experimental diffuse peak.

Difficulties arise with the intramolecular term. For polyatomic molecules, the intramolecular distances and the intermolecular ones are in the same range and it is impossible to distinguish in a spectrometer counter without energy analysis whether the scattered neutron must be attributed to an intramolecular or an intermolecular contribution. This confusion puzzled a lot of authors, mainly in liquid systems (because experiments with plastic crystals were rather scarce) until the mid-eighties: the intermolecular term was implicitly neglected and all the experimental peaks were refined with an intramolecular model, where the translation terms $T_m^* T_n$ were forgotten. Reading the papers, it is clear that this confusion can be associated with the ambiguity of the term «correlation» already mentioned.

Even if one properly takes this term into account, analysis often is still ambiguous if the two components $S_{intra}(q)$ and $S_{inter}(q)$ are not really separated by means of experiment, i.e. for sufficiently disordered systems with the scattering distributed over the whole reciprocal space.

An exception is the case when the diffuse scattering is located in a very narrow domain of the reciprocal space, as was observed by More et al [33] in CBr_4. In this case the separation of the terms is possible after a careful analysis and comparison of the calculated intramolecular and experimental scattering. But the answer is only given at the end of a long single-crystal analysis without a priori knowledge of what it will be.

Another exception is the case of diatomic molecules: they are the only system where this ambiguity always disappears, whatever the disorder should be, since the shorter bond length ($d = 1.2$ Å) produces no oscillation of the intramolecular term for q values below $q \approx 2\pi/d \approx 5.2$ Å^{-1}. In this and only this case, the answer can be known from the very beginning, since a preliminary powder experiment is sufficient to investigate the presence of a correlation peak, prior to any single crystal experiment: with oxygen, the diffuse peak at 2.3 Å^{-1} appeared clearly in powder diffraction experiment, and the data already published on nitrogen [35] also exhibit such a correlation peak. Since it includes the same distances as found in the analysis of liquid state data, this peak is at the same position as in the liquid, but with a lower intensity.

Therefore, the first fundamental and general result is that for diatomic molecules, the intramolecular and intermolecular ranges clearly separate, respectively in the high-q and low-q domains, i.e. in a simple way.

The problem is now to calculate this intermolecular correlation contribution. Within the rigid block model, the most physical way to split the correlation term in various contributions is to separate the translational and rotational degrees of freedom: three correlation terms are introduced, viz. translation-translation, rotation-rotation, and translation-rotation terms, or more simply, T–T, R–R, and T–R terms. The total scattering can be split in six terms, S_1 to S_6 [34]:

$$S_1 = \sum |\langle \beta_m \rangle|^2 [1 - |\langle T_m \rangle|^2] ;$$

$$S_2 = \sum [\langle |T_m|^2 \rangle - |\langle T_m \rangle|^2] ;$$

$$S_3 = \sum\sum \langle \beta_m^* \rangle \langle \beta_n \rangle \langle T_m^* \rangle \langle T_n \rangle \, e^{i\mathbf{q}\cdot\mathbf{R}_{mn}} ;$$

$$S_4 = \sum\sum{}' \langle \beta_m^* \beta_n \rangle [\langle T_m^* T_n \rangle - \langle T_m^* \rangle \langle T_n \rangle] \, e^{i\mathbf{q}\cdot\mathbf{R}_{mn}} ;$$

$$S_5 = \sum\sum{}' \langle T_m^* \rangle \langle T_n \rangle [\langle \beta_m^* \beta_n \rangle - \langle \beta_m^* \rangle \langle \beta_n \rangle] \, e^{i\mathbf{q}\cdot\mathbf{R}_{mn}} ;$$

$$S_6 = \sum\sum{}' [\langle \beta_m^* \beta_n T_m^* T_n \rangle - \langle \beta_m^* \beta_n \rangle \langle T_m^* T_n \rangle] \, e^{i\mathbf{q}\cdot\mathbf{R}_{mn}} ;$$

$$\mathbf{R}_{mn} \equiv \mathbf{R}_n - \mathbf{R}_m ,$$

where the summations run over the molecules of the crystal. For the double summations, the notation $\Sigma\Sigma'$ means that m and n are always different (intermolecular terms). S_1 and S_2 are the intramolecular terms associated with the translational and orientational order, respectively, i.e. $S_1 + S_2 = S_{intra}$; S_3 is the ideal long range order term without any correlation and, thus, without any real significance; S_4, S_5, S_6 are the correlation terms, respectively, the T–T term (acoustic phonons), the the R–R term and a very complex T–R term (including optic phonons).

The important result obtained by Dove and Pawley in their SF_6 Molecular Dynamics simulation is that

the S_1, S_2, S_5 are continuous in the reciprocal space, while S_4 and S_6 show both a diffuse component and a discrete component, which can be ascribed to some coherence effects, not taken into account by the S_3 term.

It is now possible to show equivalence between the experimental and calculated components. One has to split S_4 and S_6 into a diffuse term and a contribution to the Bragg lines:

$$(S_{\text{Bragg}})_{\text{exp}} = S_3 + (S_4 + S_6)_{\text{Bragg}} ,$$

$$(S_{\text{diffuse}})_{\text{exp}} = S_1 + S_2 + S_5 + (S_4 + S_6)_{\text{diffuse}} .$$

These expressions can be the starting point of a comprehensive comparison between experimental and simulation data.

Now, since we want to model the system, another question arises: what is analytically calculable ?

The evaluation of the average $\langle ... \rangle$ can be done in two ways:

(i) a numerical simulation directly produces several thousands of instantaneous configurations over which these averages are applied without any difficulty;

(ii) an analytical model needs either the knowledge of an analytical probability distribution function or a (limited) set of orientations and positions of the molecules with the corresponding weights $e^{-V_{mn}/kT}$ for each relative configurations, where $V_{mn}(\mathbf{R}_{mn}, \Omega_m, \Omega_n)$ is the potential between molecules m and n at distance $\mathbf{R}_{mn}$ and with orientations defined by Ω_m, Ω_n. Such modeling can be done for the orientation of the molecules: this is what we did for oxygen, as described in the next Section, by treating $\mathbf{R}_{mn}$ as the mean position of the molecules, i.e. neglecting the translation rotation coupling shift of the centre of mass of 6*c* molecules refined in diffraction experiment. However, the modeling of the instantaneous positions $\mathbf{R}_m$ and $\mathbf{R}_n$ of the molecules, and hence, the terms involving T_m and T_n seems far outside the possibilities of the available potentials.

So, the S_5 term can be modeled and analytically calculated, but not the S_4 and S_6 terms. Therefore, a complete analysis of diffuse scattering experiment needs numerical simulations.

Analytical model. We first decided to ignore the S_4 and S_6 terms and calculated analytically the S_5 term. We started from the best crystallographic model of disorder for both types of sites (validated by extensive cluster energy calculations) and took into account all the pairs of molecules in S_5. In order to investigate the correlation range and the correlated pairs, we reversed the sums grouping together pairs with identical configurations, equivalent via rotations of the symmetry group of the crystal, as in the usual liquid investigations. Because of the single crystal geometry and the numerous molecules and sites, the process of identifying and sorting the equivalent relative orientations is rather tedious but the result is clear:

- the only contribution that can be ascribed to an experimental result is a contribution of correlated 2*a*-6*c* molecules. This is consistent with numerical cluster calculations.
- no contribution of the 6*c*–6*c* first neighbors is found, which is not consistent with the existence of the disc-like disorder. It only means either that this contribution must be found in the neglected $S_4 + S_6$ component or maybe that the model used is not enough disordered (the molecules were located in the middle of the libration sectors).
- the calculated diffuse scattering is about 10 times too weak to explain the measurements, but for the first time it was possible to produce a calculated peak at the right place of the correlation range, as in experiment [35].
- the broad maximum of the experimental diffuse scattering can be ascribed to the intramolecular terms $S_1 + S_2$ and the sharp minimum just in the [100] direction arises from the S_5 term. Owing to the limitation of the latter term, one cannot really trust the detailed modulation in the reciprocal space. But the minimum in the vicinity of the [100] direction arises from the in-plane confinement of the 6*c* molecules. One can expect to find this feature again in the other terms.

Despite the numerous results obtained using this analytical model, the significance of the approximation made in this calculation is not clear. The main question concerning the calculated term is: what is the implication to have put the best diffraction model, i.e. to restrict the molecular orientations in the averaging procedure? In this way, we clearly added some information to the system, but an information truncated by the limited set of orientations of the statistical model: how is this information distributed among the calculated diffuse scattering contribution?

To go further, Molecular Dynamics simulation is necessary.

Simulation. A set of 512 molecules was used for this simulation. Such a box was already used in an erlier simulation by Klein et al. [36]. We used the same Lennard-Jones potential as these authors ($\varepsilon = 58$ K, $\sigma = 2.998$ Å), considered as «not the best» but a good one, able to reproduce several experimental results. The cell parameter was first estimated by Monte Carlo Metropolis with variable volume and zero pressure and $T = 50$ K. The cell parameter was found to be $a = 6.65$ Å, close to the experimental value. The Molecular Dynamics included constraints on the length of the molecules, consistent with the rigid molecule model, and used the numerical Verlet algo-

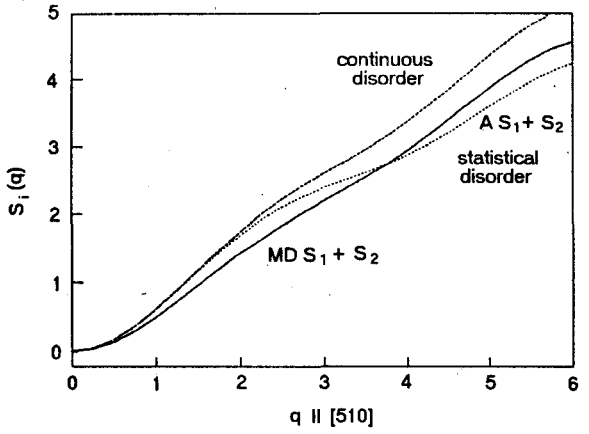

Fig. 6. Calculated diffuse scattering: intramolecular component. The vertical axis is the normalized scattering intensity (see the formula on page 150). The horizontal axis is in $a^* = 2\pi/a$ units wavenumber. The continuous line is the Molecular Dynamics calculation (MD). The dotted line is the Analytical model calculation (A). The long dashed line is the continuous disorder model.

rithm. The time step was $5 \cdot 10^{-15}$ s. After 7500 steps and stabilization of the system (T = 50.8 K) a first calculation of the S_1 to S_2 terms was performed during 10^4 steps; then another calculation 10^5 steps long was made, with the same results.

The results are shown in Figs. 6 to 9, together with the analytical model calculations described above. Because the MD S_5 value (Fig. 8) is very small, we compare MD $S_4 + S_6$ with A S_5 in Fig. 7. (MD = 2D molecular dynamics calculation, $A = 3D$ analytical model). The MD intramolecular contribution (Fig. 6) is close to that obtained in the analytical model and always lower than the continuous disorder value.

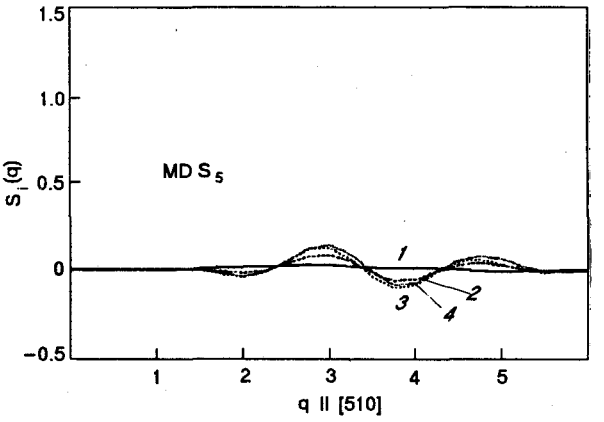

Fig. 8. Calculated diffuse scattering: intermolecular MD S_5 component for various cutoff distances (in Å): 3.4 (curve *1*); 3.9 (curve *2*); 4.5 (curve *3*); 6.1 (curve *4*). The axes as in Fig. 6. The distances to the neighbours in the *A15* structure (a = 6.65 Å) in increasing order: d_{6c-6c} = 3.34 Å, d_{2a-6c} = 3.73 Å, d_{6c-6c} = 4.07 Å, d_{2a-2a} = 5.76 Å, d_{6c-6c} = 6.22 Å (not accounted for). As the cutoff distance increases, a new shell of neighbors is added.

Several interesting results have been found for the S_4 to S_6 contributions:

- the MD S_5 term is rather small as compared to the A S_5 term;
- the MD $S_4 + S_6$ is about twice as the A S_5 term.

The contribution of various pairs can be estimated by increasing the cutoff length in the calculation of the S_1 to S_6 terms, thereby including more and more pairs in the summations (Figs. 8 and 9). Analysis shows a major contribution of the 6c-6c first neighbors, as previously expected, but the contribution of

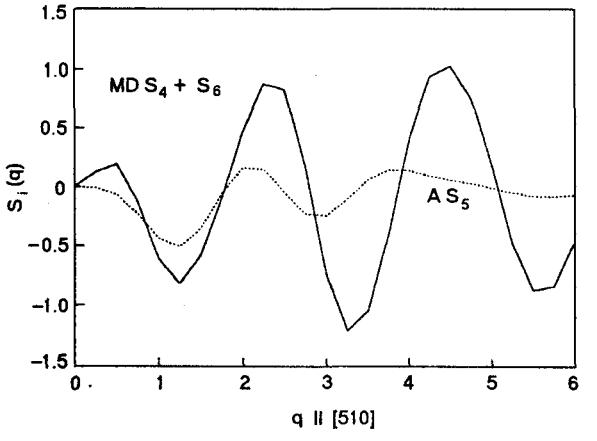

Fig. 7. Calculated diffuse scattering: intermolecular component. The axes as in Fig. 6. The continuous line is the MD $S_4 + S_6$ terms. The dashed line is A S_5 with the statistical orientation weights extracted from the best crystallographic model.

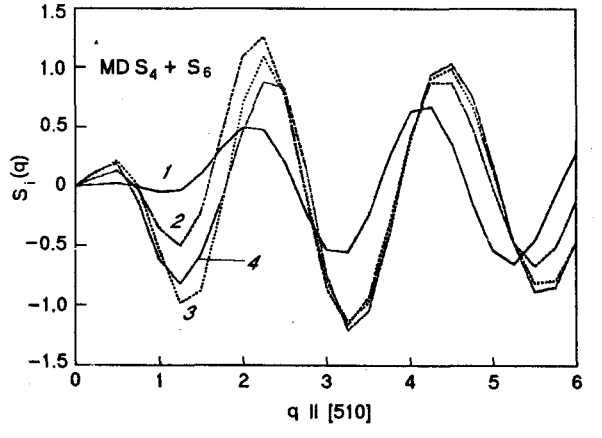

Fig. 9. Calculated diffuse scattering: intermolecular MD $S_4 + S_6$ component for various cutoff distances. The axes and notation as in Fig. 8.

the $2a$-$6c$ pairs is important, as was found in the A model. The contribution of other pairs are much smaller;

- the total MD $S_4 + S_5 + S_6$ is still unable to reproduce the experimental data. Besides, the simulated phase appears to be more disordered than the model arising from experiment. Hence, further refinements of the parameters of the model seem to be necessary.

The MD results show that the analytical model using a limited set of orientations, extracted from the best crystallographic fit, simulates part of the $S_4 + S_6$ terms. Additional work is necessary to understand clearly this effect. Most of the predictions of this model were found to be correct, so the model may be used if MD calculations are not available to at least detect a correlation term or estimate the correlation range.

4.3. Conclusion

The main results of this study can be summarized as follows.

The spherical-like $2a$ molecules are almost totally disordered, with a tendency to escape several orientations in the direction of the neighbors. The disc-like molecules perform wide librations inside angular sectors and jumps between the sectors. The correlated molecular pairs are mainly the $6c$-$6c$ nearest neighbor pairs and the $2a$-$6c$ pairs.

The interpretation of the diffuse scattering is rather delicate, since it requires for us to know how to separate the intramolecular from the intermolecular contributions in the experimental data, in order not to confuse them in the analysis. This is not possible for any molecule. Polyatomic molecules consisting of more than two atoms must produce a localized diffuse scattering. The diatomic molecules are the only systems in which severe disorder, observed in oxygen and probably in other diatomics, can be studied with a reasonable chance of success, since the peak observed in the 2–2.5 Å range is a priori known to be due to intermolecular correlations.

A complete interpretation of the diffuse scattering requires numerical simulation, since the T–T and T–R coupling terms cannot be analytically calculated.

As opposed to the numerous systems studied by Molecular Dynamics (since single crystal are not always available to perform experiment), our data on oxygen can be used to check the simulation parameters and investigate a lot of details of the disorder. Analysis is in progress to go further than the preliminary results reported here.

The analytical model, derived prior the simulation has been started, was able to predict the range of correlations between molecules and to show that the introduction of additional information through the use of a good rotational disorder model in the R–R term had the effect to simulate part of the T–T and T–R terms. So, this type of model can be used as a better approximation than just neglecting the correlation term.

5. Magnetic short range order in oxygen. Magnetic form factor

Magnetic measurements [37] showed an antiferromagnetic behavior of the low temperature α and β phases, whereas the γ and liquid phases are clearly paramagnetic.

We have performed polarized measurements in the paramagnetic and β phases, which were reported elsewhere [38,39]. We shall not reproduce here the details of these analyses but just summarize the principle of the analysis, the main results, and the general conclusions. The paramagnetic phases will be discussed together, then the β phase, and finally the form factor of the molecule, for which several problems have been encountered.

A previous polarization analysis experiment [40] showed the presence of strong antiferromagnetic correlations in the liquid phase at $T = 82$ K, far above the magnetic ordering point ($T = 24$ K). The question was whether these correlations are an intrinsic property of the oxygen molecules, or a result of the close approach of the molecules during their collisions. To choose between such models, a measurement in the solid γ phase could be enlightening: the densities of the liquid and the γ phase are close but the molecules in the solid cannot approach their neighbors as close as during a collision in the liquid.

5.1. Experimental

Using the polarization analysis method described in Sec. 3, we have measured the magnetic contributions to the neutron scattering of the magnetically disordered phases of oxygen. The q-range was 0 to 5 Å^{-1} for the liquid and γ phases and 0 to 4 Å^{-1} for the β phase. The spin flip intensity was measured separately for two orientations of the magnetic field, parallel and perpendicular to the scattering vector. Then, from the difference, an accurate separation of the magnetic scattering can be obtained, since all nonmagnetic contributions (nuclear, background, etc.) vanish. The results were normalized to $q = 0$ with the known magnetic suceptibility [37]. A broad diffuse peak can be always observed, centered around $q = 1.1$ Å^{-1} in the liquid and γ phases and around $q = 1.2$ Å^{-1} in the β phase. The scattering in the plastic γ phase is very similar to that in the liquid, but the peak is broader than in the β phase. A later experiment with gas at a pressure of 100 atm at room temperature (the density roughly 10 % of that of the condensed phases) in the 0 to 3 Å^{-1} range still

showed the same peak, centered around $q = 0.65$ Å^{-1}, though not so pronounced.

The initial question is clearly answered: strong antiferromagnetic correlations are observed in any phase and at any temperature, independently of the phase structure.

The next step is to analyze this broad peak versus the short range order in the relevant phases.

5.2. Analysis of data: paramagnetic phases

In the case of correlations, the magnetic scattering can be written for a powder sample, where the $S_{i\perp} \wedge S_{j\perp}$ cross terms vanish:

$$I_{exp}(q) = a\langle f^2(q) \sin^2 \alpha\rangle +$$

$$+ b\langle f_1(q) f_2(q) \sin\alpha_1 \sin\alpha_2 \cos(q \cdot r_{12})\rangle + \ldots$$

Here $f(q)$ is the magnetic form factor; α is the angle between the spin S and the scattering vector q, arising from the $S_\perp$ term of the diffusion amplitudes described in Sec. 4; r_{12} is the distance between the molecules 1 and 2 considered; a and b absorb all the factors, but have a precise physical meaning, since the data are normalized. $\langle\ldots\rangle$ is an average over orientations of the magnetic moments, i.e. over the $\alpha, \alpha_1, \alpha_2, \ldots$ angles and over the scattering vector orientations, due to the powder average. Other terms can be considered for further correlated neighbors.

The first term is purely paramagnetic (intramolecular term in the language of Sec.5). The other terms are intermolecular correlation terms, responsible for the decrease of the scattering and, therefore, of the magnetic susceptibility at low angles. The latter is related to the $q = 0$ scattering by

$$I_{magn}(q = 0) = \Gamma^2 kT \chi_0 / \mu_B^2 ,$$

where Γ was defined in Sec. 3 and χ_0 is the molecular susceptibility.

The general case is intricate, but analytical expressions can be derived within several approximations. The most natural, considering the known oxygen structures and the data available, is to assume antiferromagnetic correlations in order to replace $\sin\alpha_1 \sin\alpha_2$ by $\sin^2\alpha$. This allows us to find analytical expressions for the correlation term. Another problem is the possibility of a correlation between the orientations of the magnetic moment and the molecular axis. Due to the axial symmetry of the p orbital, three models have been considered in Ref. 40: a totally uncorrelated model, an Ising model with the spin parallel to the molecular axis, and a XY model with the spin normal to the molecular axis. For the γ phase, the result is no doubt to reject the Ising model with the moment parallel to the molecular axis. The difference between the totally uncorrelated model and the XY model is rather small, but the structures of low temperature phases with the moments perpendicular to the molecular axes are consistent with the XY model.

The refined distances of the first antiferromagnetically correlated neighbors are $r_{12} = 3.37$, 3.6 and 5.7 Å in the γ, liquid, and gas phases, respectively. For liquid and gas, a simple formula $I_{exp}(q) = a + b \sin qr/qr$ was used. For the γ phase, there is a strong suggestion for a correlation up to the second in-chain neighbor, under the condition that the form factor should be modified as discussed below.

5.3. The β phase

Here the problem is rather different. Many results, experimental as well as theoretical, have been accumulated for the low temperature α and β phases. Let us first review briefly these results.

The antiferromagnetic α structure consists of parallel layers, the (a,b) planes, in which the molecules stand upright, parallel to each other, as already discussed in Sec. 2. The magnetic moment lies along the b axis of the body-centered monoclinic cell, i.e. perpendicular to the molecular axis. This magnetic structure was established by the early neutron scattering experiments [4], showing two additional Bragg lines, never observed in x-ray experiments.

The magnetic short range order (SRO) of the β phase was discovered at the same time (Collins [4]): the two antiferromagnetic Bragg lines of the α phase are replaced by a broad diffuse peak of magnetic origin. Based on this first experimental result, theoretical studies were reported [41–44], all based on two facts, the rhombohedral structure and the sharp decrease of the exchange integrals with the distance between molecules [14]. Therefore, most of the theoretical models are restricted to the nearest neighbors within the hexagonal planes. More recent and elaborate $2D$ and $3D$ models [42] investigate the role of more distant molecules. Because of the theoretical difficulty to introduce directly a short range order, long range order (LRO) models are generally proposed, and the hypothesis is made that this local order is retained as SRO in the real solid. A recent paper [43] took into account a SRO nature of the correlations. On the other hand, a LRO model, the «infinitely degenerate helix» was also proposed [44]: an asymmetric saw-tooth profile arises from the superposition of an infinite set of incommensurate Bragg lines, thus associated with a pure elastic scattering.

The first experimental result in the neutron scattering experiment was obtained by Stephens et al. [5]. It was related to a triangular SRO model, with a correlation length of 3.6 Å (first neighbor: 3.3 Å).

The authors showed clearly the inelastic nature of the magnetic diffuse peak, thus excluding the purely elastic degenerate helix model. Nevertheless, their experiment was rather difficult to interpret, because of a strong nuclear background and the restricted q-range of the experiment (0.6–1.6 $Å^{-1}$). Therefore, a more precise experiment, reported in Ref. 39, was necessary in order to be able to distinguish more clearly between the theoretical models.

The puzzling discrepancy between the theoretical models and the previous experimental results put several important questions:

(i) Is the magnetic order long or short-ranged? This question was clearly answered by Stephen's experiment: the inelastic nature of the scattering (width 6 meV) rules out any LRO model. Our analysis clearly excluded the LRO infinite degenerate helix as well.

(ii) Is the local order 2D or 3D? Our data clearly favour a 2D model, without correlations between adjacent planes.

(iii) What 2D model? The triangular model of Ref. 5, although giving a good fit with experiment, is ruled out, since the calculated peak is slightly shifted from the experimental peak.

We have concluded that a helicoidal model (Fig. 10), with an angle of 140 ° between neighboring magnetic moments is most satisfactory. The correlation length, 5 Å, corresponds roughly to the second neighbors in the hexagonal plane. The magnetic moments stay in the hexagonal plane, i.e. orthogonal to the molecular axis. To interpret the data, especially at $q = 0$ and high q, we had to take into account the important purely paramagnetic component, associated with some completely disordered magnetic moments: this phase supports a paramagnetic behavior.

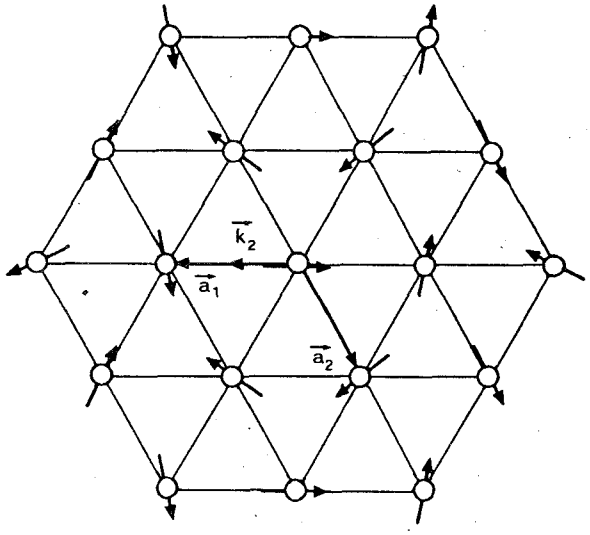

Fig. 10. Magnetic structure of β oxygen for propagation vector $k_2 = 0.393[2a^* - b^*]$ [39].

Whatever the exact value of the angle between the moments should be, the quasi-triangular SRO observed in this phase explains both neutron scattering and susceptibility results. Meier [42] showed that a LRO 2D triangular magnetic structure is destabilized by out-of-plane neighbors, while Kuchta et al. [43] showed in a beautiful paper that the $\alpha-\beta$ transition can be attributed to the magnetoelastic coupling, whereas the transition temperature ($T_{\alpha-\beta} = 24$ K), much lower than the Néel temperature ($T_N = 200$ K), can be ascribed to the triangular SRO which stabilizes the β phase.

5.4. *Molecular form factor*

In all the phases we studied, the scattering had two components: a pure paramagnetic component and a contribution of the intermolecular correlations of variable importance. The correlation contribution always disappears at high q because of the damping effect of the averaging over the $\cos(\mathbf{q}\cdot\mathbf{r}_{12})$ term. So the paramagnetic component is the only component at higher q and can be extracted from our data whatever the SRO is. This paramagnetic term, $\langle f^2(\mathbf{q})\sin^2\alpha\rangle$, is directly related to the magnetic form factor $f(\mathbf{q})$, introduced in Sec. 4 as the Fourier transform of the spin density, i.e. $|\pi_g^{\pm}|^2$. Following the analysis of Kleiner [9] and Stephens [11], the magnetic form factor can be expanded in Legendre polynomials of the angle θ_q between the molecular axis and the scattering vector $\mathbf{q}$:

$$f(\mathbf{q}) = A_0(q) - 5A_2(q)P_2(\cos\theta_q) +$$

$$+ 9A_4(q)P_4(\cos\theta_q) - \ldots$$

The radial functions $A_n(q)$ are calculated by Kleiner (or Stephens) on the basis of the Gaussian atomic orbitals of Meckler [9]. Only the A_0, A_2, and A_4 terms are significant. More elaborate developments of Meier et al. [10], based on higher (3 to 5) Gaussian orbitals and the Stewart series expansions, give similar results. These expressions were explicitly introduced in the $\langle\ldots\rangle$ integrals previously mentioned.

In all the phases, the refinements remained rather poor at high q, with the calculated paramagnetic scattering always smaller than the experimental one. Since these high q data are close to the first zero of $A_0(q)$, the predominant terms are the next radial functions. A phenomenological model, obtained by multiplying arbitrarily the radial integrals $A_2(q)$ and $A_4(q)$ by a constant factor ζ, substantially improved all the refinements at high q. An interesting result is that the same coefficient ($\zeta \approx 1.4$) was appropriate for

the β, γ, and liquid phases. Moreover, it did not modify the hierarchy of the various correlation models [39,40], which show that we are really faced with a problem in the calculated form factor itself and not with some artefacts introduced through the correlation term analysis. What is the meaning of this phenomenological multiplying factor? We are led to the hypothesis that the calculated A_2 and A_4 integrals are probably underestimated. Other contributions to such a discrepancy such as multiple scattering or polarization efficiency have been discussed [39] and found negligible. Using the expansion of the spin density [11], one can write the radial integral as

$$A_{2l}(q) = \int dr\, r^4 \exp(-2br^2)\, j_{2l}(qr)\, \varphi_{2l}(r)\,,$$

where $\varphi_{2l}(r)$ can be analytically expressed in terms of modified spherical Bessel functions. Both $\varphi_{2l}(r)$ and the spherical Bessel function $j_{2l}(qr)$ are growing functions of radius in the relevant qr domain. Clearly, an increase of the radial integral $A_{2l}(q)$ can result from an increase of the radial expansion of the atomic orbitals. In a description of the π orbitals better than only the $2p$ atomic orbitals considered until now, an expansion of the basis of atomic orbitals by adding atomic orbitals with wider radial extension would also lead to the result of increasing the A_2 and A_4 radial integrals. Whatever the real mechanism, a new theoretical approach of representing the magnetic factor with more reliable expressions in the π orbitals seems highly desirable.

Conclusion

Oxygen exhibits strong antiferromagnetic correlations in the paramagnetic domain, but they remain limited to the closest neighbors. In contrast to the classical magnetic systems, showing various LRO phases, we have here a unique LRO phase, as well as an evolution of the SRO through the phase transitions associated with the onset of orientational and translational disorder. We believe that the Meckler wave function should be improved to better represent the magnetic form factor in the high-q domain.

The plastic phase of oxygen exhibits an $A15$ structure with two distinct disorders, due to the possibility to form linear chains of molecules at closer contact than in the hexagonal structure observed for nitrogen. Diffraction, magnetic and nuclear diffuse scattering experiments produced a lot of new results for this phase. As shown by single crystal diffraction, the molecules in the chains ($6c$ sites) rotate within the planes orthogonal to the chain axis, performing large librations of roughly 40° and jumps across the forbidden ⟨100⟩ and ⟨110⟩ orientations outside the 10^{-13} s time-scale accessible to neutron scattering experiments. These molecules are both orientationally and antiferromagnetically correlated as shown by diffuse scattering. The other molecules ($2a$ sites) rotate quite freely with indications that they avoid the ⟨100⟩ and ⟨120⟩ unfavorable orientations. They were found to be purely paramagnetic, without correlations of their magnetic moments with the neighbors, but rather strongly orientationally correlated with their twelve $6c$ neighbors arranged in a quasi-icosahedral symmetry that we believe to persist in the liquid.

More generally, it was found that oxygen can be considered as a model compound for pure van der Waals interaction. As to the posibility to study the $A15$ phase, characteristic of quadrupolar-free interactions, oxygen is the only compound accessible at zero pressure, for which large single crystals can be grown, allowing various experiments.

Analysis of diffuse scattering has shown that diatomics are very interesting compounds for the investigation of the total scattering through a direct comparison between experiment and simulation, since the intramolecular single-particle scattering and the intermolecular correlation scattering are well separated in reciprocal space, thus allowing a less ambiguous interpretation of the experimental data than for molecules with more than two atoms. Once again, oxygen is rather unique since the closer approach of the molecules allowed by the $A15$ structure and the two types of orientational disorder are the origin of a rather highly correlated system and a wide variety of problems to be studied.

Aknowledgements

It is a real pleasure to thank here Prof. Mikhail Strzhemechny from the Verkin Institute for Low Temperature Physics in Kharkov for his critical reading of the manuscript and comments.

1. A. F. Prikhot'ko, Yu. G. Pikus, and L. I. Shanskii, *JETP Letters* **32**, 287 (1980); A. F. Prikhot'ko, Yu. G. Pikus, L. I. Shanskii, and D. G. Danilov, *JETP Letters* **42**, 251 (1985); I. N. Krupskii, A. I. Prokhvatilov, Yu. A. Freiman, and A. I. Erenburg, *Sov. J. Low Temp. Phys.* **5**, 130 (1979).
2. J. H. Jordan, W. E. Streib, and W. N. Lipscomb, *Acta Cryst.* **17**, 777 (1964); *J. Chem. Phys.* **41**, 760 (1964).
3. D. E. Cox, E. J. Samuelsen, and K. H. Bechürts, *J. Physique* **32**, C582 (1971); *Phys. Rev.* **B7**, 3102 (1973).
4. M. F. Collins, *Proc. Phys. Soc.* **89**, 415 (1966); R. A. Alikhanov, *JETP Lett.* **5**, 349 (1967).
5. P. W. Stephens, R. J. Birgeneau, C. F. Majkrzak, and G. Shirane, *Phys. Rev.* **B28**, 452 (1983); P. W. Stephens and C. F. Majkrzak, *Phys. Rev.* **B33**, 1 (1986).
6. M. Kotani, Y. Mizuno, K. Kayama, and F. Ishiguro, *J. Phys. Soc. Jpn.* **12**, 707 (1957).
7. M. Tinkham and M. W. P. Strandberg, *Phys. Rev.* **97**, 937; 951 (1955); H. Christensen and L. Veseth, *J. Mol. Spectrosc.* **72**, 438 (1978).
8. P. H. Krupenie, *J. Phys. Chem. Ref. Data* **1**, 423 (1972).
9. W. H. Kleiner, *Phys. Rev.* **97**, 411 (1955) (based on atomic Gaussian orbitals from A. Meckler, *J. Chem. Phys.* **21**, 1750 (1953)).

10. R. J. Meier and R. B. Helmholdt, *Phys. Rev.* **B29**, 1387 (1984) (based on series developments from R. F. Stewart, *J. Chem. Phys.* **50**, 2485 (1969); **51**, 4569 (1969)).
11. P. W. Stephens, *Phys. Rev.* **B31**, 4491 (1985).
12. R. F. W. Bader and W. H. Henneker, *J. Chem. Phys.* **46**, 3341 (1967); A. C. Wahl, *Science* **151**, 961 (1966).
13. D. E. Stogryn and A. P. Stogryn, *Mol. Phys.* **11** , 371 (1966); the polarizability is given by J. O. Hirshfelder, C. F. Curtis, and R. B. Bird, *Molecular Theory of Gases and Liquids*, Wiley (1954), p. 950.
14. M. C. Van Hemert, P. E. S. Wormer, and A. Van der Avoird, *Phys. Rev. Lett.* **51**, 1167 (1983); P. E. S. Wormer, and A. Van der Avoird, *J. Chem. Phys.* **81**, 1929 (1984); R. J. Meier, C. J. Shinkel, and A. de Visser, *J. Phys. C : Solid State* **15**, 1015 (1982).
15. V. A. Slyusarev, Yu. A. Freiman, and R. P. Yankelevitch, *Sov. J. Low Temp. Phys.* **10**, 113 (1984).
16. J. C. Laufer and G. E. Leroi, *J. Chem. Phys.* **55**, 933 (1971).
17. O_2 phase diagrams: D. Shiferl, D. T. Cromer, and R. L. Mills, *Acta Cryst.* **B37**, 1329 (1981); **B39**, 153 (1983); B. Olinger, R. L. Mills, and R. B. Roof Jr., *J. Chem. Phys.* **81**, 5068 (1984). Phase diagrams of N_2 and CO: R. L. Mills, B. Olinger, and D. T. Cromer, *J. Chem. Phys.* **84**, 2837 (1986); R. L. Mills and A. F. Schuch, *Phys. Rev. Lett.* **23**, 1154 (1969); A. F. Schuch and R. L. Mills, *J. Chem. Phys.* **52**, 6000 (1970); D. T. Cromer, D. Schiferl, R. Le Sar, and R. L. Mills, *Acta Cryst.* **C39**, 1146 (1983).
18. T. H. Jordan, W. E. Streib, and W. N. Lipscomb, *J. Chem. Phys.* **41**, 760 (1964); L. Meyer, C. S. Barret, and S. C. Greer, *J. Chem. Phys.* **49**, 1902 (1968).
19. C. A. English and J. A. Venables, *Proc. Roy. Soc. (London)* **A340**, 57 (1974).
20. A. P. Brodyanskii and Yu. A. Freiman, *Sov. J. Low Temp. Phys.* **12**, 684 (1987).
21. J. E. Cahill and G. E. Leroi, *J. Chem. Phys.* **51**, 97 (1969); H. Kiefte, M. J. Clouter, N. H. Rich, and S. F. Ahmad, *Chem. Phys. Lett.* **70**, 425 (1980); K. D. Bier, and H. J. Jodl, *J. Chem. Phys.* **81**, 1192 (1984).
22. F. Dunstetter, *Ph.D. Thesis*, Université de Paris-Sud, Orsay, France (1988).
23. O. Halpern and M. R. Johnson, *Phys. Rev.* **55**, 898 (1939).
24. R. M. Moon, T. Riste, and W. C. Koehler, *Phys. Rev.* **181**, 920 (1969).
25. F. Dunstetter and A. Delapalme, *Physica* **B156–157**, 112 (1988).
26. W. Press and A. Hüller, *Acta Cryst* **A29**, 252; 257 (1973); *Acta Cryst.* **A35**, 876 (1979).
27. C. Von der Lage and H. A. Bethe, *Phys. Rev.* **71**, 612 (1947); extended by D. Bell, *Rev. Mod. Phys.* **26**, 311 (1954).
28. S. L. Altmann, C. J. Bradley, and A. P. Cracknell, *Rev. Mod. Phys.* **37**, 19; 33 (1965).
29. F. Coppens, N. K. Hansen, and E. D. Stevens, *Isr. J. Chem.* **16**, 159; 163; 175 (1977).
30. K. Kurki-Suonio and V. Meisalo, *Ann. Acad. Sci. Fennicae* **A241**, 3 (1967); M. Kara and K. Kurki-Suonio, *Acta Cryst.* **A37**, 201 (1981) and references therein.
31. W. Press, H. Grimm, and A. Hüller, *Acta Cryst.* **A35**, 881 (1979); K. D. Ehrenhardt, W. Press, and G. Heger, *Acta Cryst.* **B39**, 171 (1983).
32. G. Dolling, B. M. Powell, and V. F. Sears, *Mol. Phys.* **37**, 1859 (1979).
33. M. More, J. Lefebvre, B. Hennion, B. M. Powell, and C. M. E. Zeyen, *J. Phys.* **C13**, 2833 (1980).
34. M. T. Dove and G. S. Pawley, *J. Phys C : Solid State* **17**, 6851 (1984).
35. B. M. Powell, H. F. Nieman, and G. Dolling, *Chem. Phys. Lett.* **75**, 148 (1980); *J. Chem. Phys.* **79**, 982 (1983).
36. M. L. Klein, D. Levesque, and J, J. Weis, *Phys. Rev.* **B21**, 5785 (1980).
37. G. de Fotis, *Phys. Rev.* **B23**, 4714 (1981).
38. F. Dunstetter, V. P. Plakhty, and J. Schweizer, *J. Mag. Mag. Mat.* **96**, 282 (1991).
39. F. Dunstetter, V. P. Plakhty, and J. Schweizer, *J. Mag. Mag. Mat.* **72**, 258 (1988).
40. M. Deraman, J. C. Dore, and J. Schweizer, *J. Mag. Mag. Mat.* **50**, 178 (1985).
41. V. M. Loktev, *Sov. J. Low Temp. Phys.* **5**, 142 (1979); V. A. Slyusarev, Yu. A. Freiman, and R. P. Yankelevich, *JETP Lett.* **30**, 270 (1979); *Sov. J. Low Temp. Phys.* **7**, 265 (1981); R. D. Etters, A. A. Helmy, and K. Kobashi, *Phys. Rev.* **B28**, 2166 (1983).
42. R. J. Meier, *Phys. Letters* **107A** (1985), 275; **12A**, 341 (1985); A. P. J. Jansen, *Phys. Rev.* **B33**, 6352 (1986).
43. B. Kuchta, T. Luty, and R. J. Meier, *J. Phys. C: Solid State Phys.* **20**, 585 (1987).
44. E. Rastelli and A. Tassi, *J. Phys C: Solid State Phys.* **19**, L423 (1986); **21**, 1003 (1988).